東北大学

平成２４年１２月１１日

報道機関　各位

国立大学法人東北大学

【制振技術】と【エネルギーハーベスティング】を同時実現する
完全セルフパワード制振技術の実証に成功
（独創的な自給自足型の無電源制振技術による「振動制御装置」の開発）

＜概要＞

東北大学の槙原幹十朗准教授は（航空宇宙工学)、高度な振動制御演算を行う独創的なデジタルマイクロプロセッサーシステムを設計し、これを用いて振動制御に外部電源供給が不要な、セルフパワード制振の「振動制御装置」を開発しました。圧電素子を装置に組込み、変形させると電圧を発生する圧電効果と、電圧がかかると変形する逆圧電効果の、両方を効果的に作動させることで実現しました。従来の外部電源が不要な振動制御は、単純波形の単調な振動しか抑制できず、複雑波形の振動を抑制するには、外部電力が必要でした。本開発は、複雑波形の振動抑制においても外部電源を不要とし、振動抑制に成功しました。

圧電素子に、制御器からの信号で切替るスイッチ回路（デジタルマイクロプロセッサーシステム）を取付けることで、従来課題を解決しました。プロセッサーが高度なデジタル演算を行い、移動体構造の複雑波形の振動に最適に対応する機能を持ちます。更に、振動から電気エネルギーを取出し、デジタルプロセッサーの駆動にも電力を供給する等、電力の自己完結機能を有する独創的な開発です。電気的に自立型の自家発電振動制御システムを構築しました。高度なデジタルプロセッサーの演算機能により、複雑振動から電気エネルギーを取出す【エネルギーハーベスティング】と、【振動制御】の両方を可能にしました。

コンパクトな設計の自立型振動制御システムは、電源不要で従来のバッテリー交換も不要です。小型振動制御装置は、実用化において安価の強みがあり、構造物に多数個の分散配置で集中制御機能が不要

な「ユビキタス制振システム」が可能になります。デジタルマイクロプロセッサー回路の、スイッチの切換えのみで振動抑制される原理より万一、制御振動が誤って振動が大きくなる等の不安定要素は皆無です。　現実的には、単調振動の構造はほとんどなく、多くは複数振動が重ね合わさる複雑振動です。本開発は電源不要で、振動をひとつの圧電素子で８割抑制することを実証しました。複雑な振動を要しながらも、外部電源・ケーブル不要な「振動抑制装置」として、デジタルマイクロプロセッサー回路のスイッチ切換えのみで作動する画期的な開発として期待されます。　実用化において、外部電源に頼れない構造物等の振動制御に適用できます。また、タイヤ・タービン等の回転体に有用です。更に航空機・電車・自動車・長い橋梁・防音壁等、多くの身近な分野での実用化が期待されます。

■用途の応用発展・可能性■

航空機：①機内電源に利用　②機内へのエンジン轟音の透過低減に利用

電　車：①車体・台車部分の振動制御に利用　②車軸状態のモニタリング送信電源に利用

自動車：①タイヤ振動を車内電源に利用　②車体・台車部分の振動制御に利用

長い橋梁：①モニタリング発信装置の電源利用　②橋梁の重要部の振動制御に利用

防音壁　：①高速道路の防音壁が受ける振動を、道路モニタリング情報の送信電源に利用
　　②防音壁の騒音透過低減に利用

この成果は、「２０１２年９月アメリカ航空宇宙学会誌（AIAA　Journal）」に掲載されました【添付】。

※ＪＡＸＡとの衛星・ロケットの振動制御に尽力し、現在ＪＡＸＡ客員准教授　兼務での共同開発です。重要なスイッチ回路部分の独創的なデジタルプロセッサーシステムは、東北大学の槙原幹十朗准教授の設計によるものです。

【概念図】

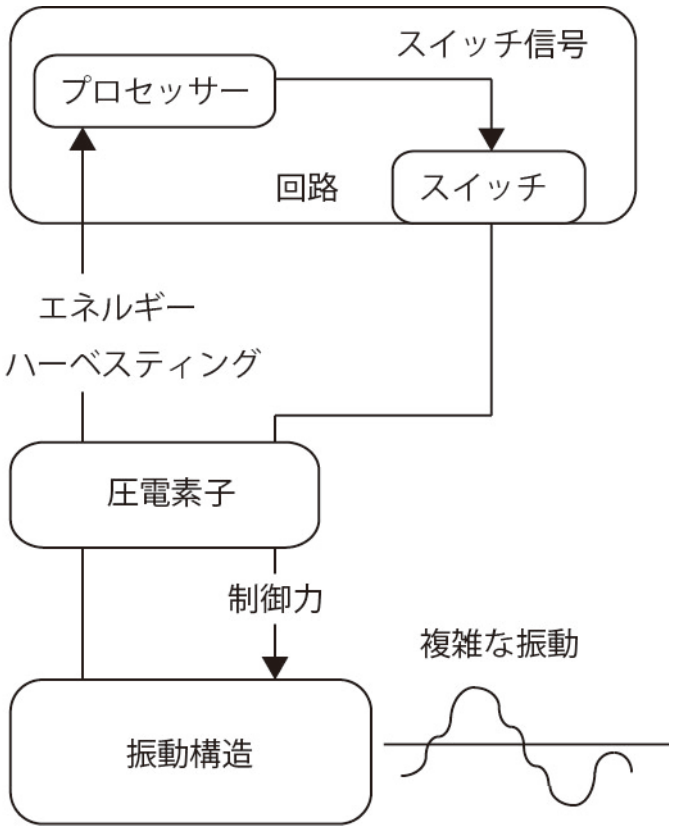

（お問合せ先）

東北大学大学院工学研究科　航空宇宙工学専攻

槙原幹十朗　准教授（makihara@ssl.mech.thohoku.ac.jp）

担当：東北大学　産学連携推進本部　リエゾン

産学連携コーディネーター

芝山多香子（shiba@rpip.tohoku.ac.jp）

電話番号：022-217-6044

AIAA JOURNAL
Vol. 50, No. 9, September 2012

Innovative Digital Self-Powered Autonomous System for Multimodal Vibration Suppression

Kanjuro Makihara*
Tohoku University, Sendai 980-8579, Japan
and
Shinsuke Takeuchi,† Shigeru Shimose,‡ and Junjiro Onoda§
Japan Aerospace Exploration Agency, Kanagawa 252-5210, Japan

DOI: 10.2514/1.J051560

A novel invention, a digital self-powered autonomous system, is proposed to achieve sophisticated vibration suppression dealing with multimodal vibrations. This vibration suppressor can be used ubiquitously at any site because it does not require an external power supply or a central control authority. The digital approach enables the system to be programmed, and thus, it affords some versatility with regard to control schemes. The proposed system is a vast improvement over conventional analog-autonomous systems whose fine-tuning is very difficult. The digital unit can be implemented in multi-input/multi-output systems to suppress complicated structural vibrations, such as multimodal vibrations. This paper provides an analytical discussion on the energy-harvesting effect on suppression performance in terms of the power balance and flow. Experiments demonstrate that the vibration magnitude reduces dramatically by as much as 79.7% under force excitation, although the self-powered control unit is used.

Nomenclature

a = displacement amplitude of the single-degree-of-freedom system
$\mathbf{B}_p$ = input matrix
b_p = piezoelectric constant of piezoelectric transducer
C_p = constant-strain capacitance
$\mathbf{C}_p$ = constant-strain-capacitance matrix
C_s = storage capacitance
$\mathbf{D}$ = damping matrix
$\mathbf{F}$ = positive feedback gain matrix
f_p = tensile force exerted on piezoelectric transducer
$\mathbf{K}$ = constant-charge-stiffness matrix
k_p = constant-charge stiffness of piezoelectric transducer
$\mathbf{M}$ = mass matrix
m = mass of the single-degree-of-freedom system
Q = electric charge applied to piezoelectric transducer
Q_T = switching criteria for semi-active control
s_1, s_2 = parameters for Kalman filter design
$\mathbf{u}$ = displacement vector
u_1, u_2 = displacements of upper mass and lower mass
V_p = voltage applied to piezoelectric transducer
V_s = storage voltage in storage capacitor
V_{sen} = voltage of piezoelectric sensor
W_{excited} = input power of vibration excitation through a vibration shaker
W_h = power harvested via diode bridge
W_r = power dissipated by a resistor
W_{without} = power dissipated without energy harvesting
$\mathbf{w}$ = external force vector
w_1, w_2 = controller design parameters
x_1 = elongation of piezoelectric transducer
α = control gain for direct-velocity-feedback method
β = modal combination parameter for vibration excitation
γ = magnitude of vibration excitation
ζ = modal damping coefficient
ζ_c = damping coefficient for electric circuit
η = overshoot ratio of piezoelectric voltage
$\boldsymbol{\xi}$ = modal displacement vector
ω = natural frequency of the single-degree-of-freedom system
ω_c = natural frequency of electric circuit resonance
ω_k = natural frequency of kth vibration mode
$\hat{\cdot}$ = estimated value by the Kalman filter
$\cdot_{\mathrm{ex}}$ = experimental setup parameters

I. Introduction

A NUMBER of studies have exploited the piezoelectric and converse piezoelectric effect in the synthesis of piezoelectric materials and electric devices to suppress structural vibrations [1–3]. The piezoelectric effect is the generation of voltage as a result of external forces or material deformation, and is usually exploited in sensor applications [4,5]. In contrast, the converse piezoelectric effect generates forces and deforms the material as a result of an applied electric charge or voltage, and is often exploited in actuator applications [6]. As these effects are reversible, mechanical and electrical energy can be generated cyclically in piezoelectric materials.

Passive vibration suppression is commonly used because it is easy to implement. However, because passive systems cannot adapt to environmental changes, suppression performance may deteriorate when the design parameters drift from optimally tuned values [7]. Therefore, to achieve high suppression performance, researchers have been working on various active-vibration-suppression systems. Although an active vibration control system usually provides a satisfactory performance, in general, it is costly and its reliability is reduced because of unstable control phenomena, such as spillover. Thus, it may be desirable to adopt a semi-active suppression system to avoid the disadvantages of active systems. A semi-active system attenuates vibrations by changing the states of the structure with

Presented as Paper 2011-1785 at the 52nd AIAA/ASME/ASCE/AHS/ASC Structures, Structural Dynamics, and Materials Conference, Denver, CO, 4–7 April 2011; received 16 August 2011; revision received 14 December 2011; accepted for publication 1 February 2012.

*Associate Professor, Department of Aerospace Engineering, 6-6-01 Aramaki-Aza-Aoba, Aoba-ku; makihara@ssl.mech.tohoku.ac.jp. Member AIAA.

†Assistant Professor, Institute of Space and Astronautical Science, 3-1-1 Yoshinodai, Sagamihara. Member AIAA.

‡Senior Researcher, Institute of Space and Astronautical Science, 3-1-1 Yoshinodai, Sagamihara. Member AIAA.

§Director General, Institute of Space and Astronautical Science, 3-1-1 Yoshinodai, Sagamihara. Associate Fellow AIAA.

a variable element, such as variable stiffness or damping force. Because the semi-active suppression system exploits passive mechanisms, it guarantees system stability even in the event of control system malfunction.

Semi-active systems do not require any external energy to suppress vibrations, but do require peripheral devices, such as external controllers, sensors, and AD/DA boards, which consume a substantial amount of electrical energy. To avoid the necessity of external energy, analog self-powered systems based on a semi-active approach have been proposed [8–10]. These systems do not require any external power supply or control authority. However, analog circuit systems are rather impractical because it is difficult to finely tune various parameters and impossible to program the systems. In addition, analog systems cannot handle situations wherein certain parameters are to be changed on account of modifications to the system.

A digital self-powered autonomous vibration suppressor has been developed, featuring sophisticated vibration suppression, to alleviate the disadvantages of analog self-powered systems. The significance and definition of the sophisticated vibration controls are described elaborately in [11]. The proposed unit consists of a programmable microprocessor, a piezoelectric transducer, an energy-harvesting section, an inductor, and a selector switch. In particular, the self-powered processor changes the electric switch automatically in sync with the vibration phase, and, therefore, the unit can achieve autonomous vibration suppression. The multifunctional, self-controlled processor is driven only by the voltage of the piezoelectric transducer via the energy-harvesting section, which means that the unit is completely isolated in terms of energy flow. In other words, no external energy is required to activate the sensors, processors, switches, and transducers that will suppress even complicated multimodal vibrations. The piezoelectric transducer works as a semi-active vibration-suppressing actuator and as a power supply to drive the microprocessor. As will be described in detail, the self-powered vibration suppressor has an energy-harvesting section to supply electrical energy to the microprocessor. It exploits both the energy-recycling vibration-suppression mechanism [12–14] and the energy-harvesting mechanism [15].

In this paper, the energy-recycling mechanism and its switching circuit are first described, followed by the addition of an energy-harvesting device to the energy-recycling switching circuit. Vibration-suppression experiments are carried out to validate the digital autonomous self-powered suppressor system. All of the digital operating procedures in one clock cycle are described. The details of the controller designing are presented. Then, single-modal vibration-suppression experiments are undertaken, and the displacement and voltage under no-control and self-powered control conditions are compared. Multimodal vibration-suppression experiments are carried out. Last, the advantages of digital self-powered autonomous system over conventional systems are discussed.

II. Theoretical Analysis of Harvesting Influence on Suppression Performance

An energy-recycling semi-active approach was adopted [12–14] in light of its high reliability and energy efficiency. The energy-recycling method inherently possesses energy-harvesting [15] and energy-confinement mechanisms [16], making it superior to conventional semi-active methods for various applications (e.g., vibration suppression of an artificial satellite [17]). Depending on the switching strategy and circuit components employed, this energy-recycling semi-active approach is known as synchronized switch damping on inductor, LR-switching, RL-shunt, and so on. Qiu et al. [18] have presented an extensive latest overview of this field (i.e., switching-control approaches using piezoelectric materials for vibration suppression) that enables readers to quickly grasp the history and significance of semi-active vibration suppression.

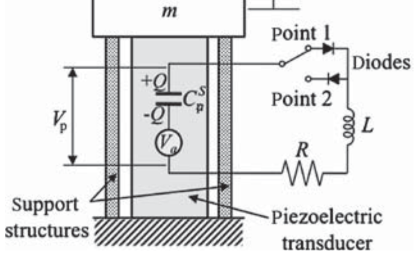

Fig. 1 SDOF system with a switching circuit for the energy-recycling mechanism.

A. Single-Degree-of-Freedom Model with Energy-Recycling Circuit

A simple single-degree-of-freedom (SDOF) system (shown in Fig. 1) was considered that is composed of a mass and a piezoelectric transducer. The piezoelectric transducer comprises multiple layers of a piezoceramic material, and it generates an axial force. The linear relation among the tensile load f_p exerted on the transducer, the elongation x_1 of the transducer, and electric charge Q, and the corresponding relation with the piezoelectric voltage V_p can be written as

$$f_p = k_p x_1 - b_p Q \tag{1}$$

$$V_p = -b_p x_1 + Q/C_p \tag{2}$$

The values of k_p, b_p, and C_p are functions of the size and characteristics [19] of the piezoceramic. From Eq. (1), the equation of motion of this system can be written as

$$m\ddot{x}_1 + k_p x_1 = b_p Q \tag{3}$$

If an active-control method is used, the vibrations of the structure can be suppressed by supplying a control input charge Q_T to the piezoelectric transducer according to the state of the system. A number of active-control theories can be used to obtain the value of Q_T. Simple active-control logic is the direct-velocity-feedback approach [20]:

$$Q_T = -\alpha \dot{x}_1 \tag{4}$$

in which α is the control gain ($\alpha > 0$). The authors attempt to semi-actively suppress the vibration of the structure by switching the circuit connection point instead of actively supplying a control charge or voltage to the actuators. Therefore, in the semi-active approach, Q_T is used as the switching criterion.

To implement semi-active vibration suppression based on energy recycling, the piezoelectric transducer is shunted on a switching circuit composed of a selector switch, a resistor, and an inductor (Fig. 1). It can be seen that when the electric current flows

$$L\ddot{Q} + R\dot{Q} + Q/C_p = b_p x_1 \tag{5}$$

and when the electric current does not flow

$$\dot{Q} = 0 \tag{6}$$

Thus, Eqs. (2) and (5) can be rewritten as

$$L\ddot{Q} + R\dot{Q} = -V_p \tag{7}$$

To understand how the semi-active control works, it can be assumed that the amplitude of the vibration of the system is almost constant even when this semi-active control is applied. The mass motion is assumed as

$$x_1 = a\cos(\omega t) \tag{8}$$

The value of Q can be made as large (positive) as possible when Q_T is positive, and as small (negative) as possible when Q_T is negative. It is clear from Eqs. (6) and (7) that when the selective switch is connected properly, Q starts to increase if $V_p < 0$, and to decrease if $V_p > 0$.

Owing to the two diodes, the switching logic is constructed [14] as follows. Turn the switch to point 1 when $Q_T < 0$ and to point 2 when

$$Q_T > 0 \tag{9}$$

It can be assumed that the displacement of the mass during the very short period when the value of Q changes is small, and that the displacement can be approximated as $x_1 = a$. Then, the following equation can be derived from Eq. (5):

$$Q = ab_pC_p - ab_pC_p\exp(-\zeta_c\omega_c t)\left[\cos(\omega_c\sqrt{1-\zeta_c}t) + \frac{\zeta_c}{\sqrt{1-\zeta_c}}\sin(\omega_c\sqrt{1-\zeta_c}t)\right] \tag{10}$$

in which

$$\omega_c \equiv \frac{1}{\sqrt{LC_p}}, \qquad \zeta_c \equiv \frac{R}{2L\omega_c} \tag{11}$$

The inversion of electric charge and subsequent voltage inversion are notable characteristics of the energy-recycling mechanism.

B. Energy Analysis of Energy-Harvesting Effect on Self-Powered System

An energy-harvesting device was then added to the energy-recycling switching circuit. The switching-control system that includes the diode bridge is shown in Fig. 2. Here, the authors analyze theoretically the harvesting influence on the suppression performance of the self-powered system. The harvesting device is composed of a diode bridge and an electric load (i.e., a capacitor C_s). The authors focus on the value of the piezoelectric voltage in two systems: with and without the harvesting device, and assume that the value of C_s is much larger than that of C_p. Figure 3 shows a schematic illustration of the piezoelectric voltage histories in the system in Fig. 2 with and without energy harvesting. The system with energy harvesting has a circuit that is connected to the diode bridge as depicted in Fig. 2, whereas the system without energy harvesting has a circuit that is not connected to the diode bridge. The value of the piezoelectric voltage immediately after the voltage inversion finishes

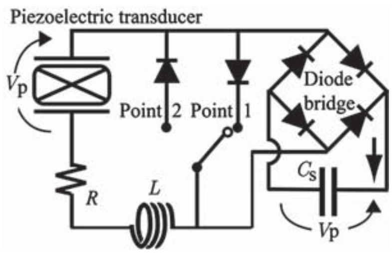

Fig. 2 Switching circuit with the energy-harvesting device.

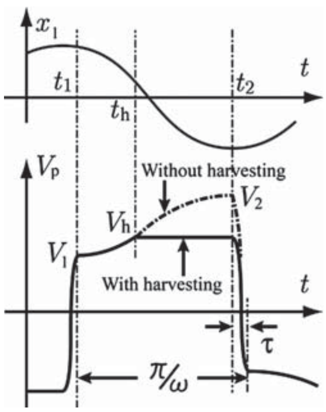

Fig. 3 Schematic illustration of the piezoelectric voltage with and without harvesting.

is defined as V_1 at $t = t_1$. In the system without an energy-harvesting device, the peak voltage is V_2 at $t = t_2$. On the other hand, in the system with the energy-harvesting device, the piezoelectric voltage increases to V_h at $t = t_h$, and remains constant until $t = t_2$ because V_p and V_s are balanced. The constant voltage V_h results from power outflow through the diode bridge. The overshoot ratio of the inverted voltage η can be defined as

$$\eta \equiv \frac{V_1}{V_h} \tag{12}$$

From Eq. (2), considering that Q is constant at t_1 and t_2, Eq. (13) is obtained:

$$V_2 - V_1 = 2ab_p \tag{13}$$

The averaged power that is harvested via the diode bridge W_h can be written as

$$W_h = \frac{\omega C_p V_h(V_2 - V_h)}{\pi} \tag{14}$$

For simplicity, the normalized parameters are introduced:

$$v_1 \equiv \frac{V_1}{2ab_p}, \qquad v_2 \equiv \frac{V_2}{2ab_p}, \qquad v_h \equiv \frac{V_h}{2ab_p}, \qquad w_h \equiv \frac{\pi}{(2ab_p)^2C_p\omega}W_h \tag{15}$$

Then, the following relations are obtained:

$$v_1 = \eta v_h \qquad v_2 - v_1 = 1 \qquad w_h = v_h(v_2 - v_h) \tag{16}$$

The equation for v_h is

$$(1-\eta)v_h^2 - v_h + w_h = 0 \tag{17}$$

Considering that $v_2 = v_h$ at $w_h = 0$, v_h is

$$v_h = \frac{1 + \sqrt{1 - 4w_h(1-\eta)}}{2(1-\eta)} \tag{18}$$

Thus, the following relation is obtained:

$$\frac{V_h}{V_2} = \frac{v_h}{v_2} = \frac{1 + \sqrt{1 - 4w_h(1-\eta)}}{2 - \eta + \eta\sqrt{1 - 4w_h(1-\eta)}} \tag{19}$$

The dissipated energy owing to the current flow through the resistor R in Fig. 2 at each switching event can be expressed as

$$\frac{1}{2}C_p(V_h^2 - V_1^2) = \frac{1}{2}C_p(ab_p)^2(1-\eta^2)\left\{\frac{1 + \sqrt{1 - 4w_h(1-\eta)}}{1-\eta}\right\}^2 \tag{20}$$

Because the switching occurs every π/ω seconds, the dissipated power in the resistor W_r is given by

$$W_r = \frac{\omega}{2\pi}C_p(ab_p)^2(1-\eta^2)\left\{\frac{1 + \sqrt{1 - 4w_h(1-\eta)}}{1-\eta}\right\}^2 \tag{21}$$

The mechanical vibration energy is transformed into electrical energy via the piezoelectric transducer and is transferred to the electric circuit. For the steady-state condition, the transferred power, which is the deprived vibration power, is equal to the sum of the harvested power flowing into an electrical load and the dissipated power in the resistor. Accordingly, for the steady-state condition, the total deprived power of the vibration system is

$$W_h + W_r = \frac{\omega}{2\pi}(ab_p)^2 C_p\left[\left(\frac{1+\eta}{1-\eta}\right)\left\{1+\sqrt{1-4w_h(1-\eta)}\right\}^2 + 8w_h\right] = \frac{\omega}{\pi}(ab_p)^2 C_p\left[\left(\frac{1+\eta}{1-\eta}\right)\left\{1+\sqrt{1-4w_h(1-\eta)}\right\} + 2(1-\eta)w_h\right] \tag{22}$$

Equation (22) indicates the performance of vibration suppression with the energy-harvesting device, because vibration suppression is inherently involved in depriving vibrating structures of vibrational energy. In a system without an energy-harvesting device, the harvested power W_h is 0 W. Without energy harvesting, the deprived power W_{without} is obtained from Eq. (21) by substituting $w_h = 0$:

$$W_{\mathrm{without}} = \frac{2\omega}{\pi} C_p (ab_p)^2 \left(\frac{1+\eta}{1-\eta}\right) \tag{23}$$

This equation indicates the performance of vibration suppression without the energy-harvesting device. When electrical power is used for the energy-harvesting mechanism, the total power for the vibration system is reduced by

$$W_{\mathrm{without}} - (W_h + W_r) = \frac{\omega}{\pi}(ab_p)^2 C_p\left[\left(\frac{1+\eta}{1-\eta}\right)\{1 - \sqrt{1-4w_h(1-\eta)}\} - 2(1-\eta)w_h\right] \tag{24}$$

In the case that $w_h \ll 1$, Eq. (24) approximates

$$W_{\mathrm{without}} - (W_h + W_r) \approx \frac{4\omega}{\pi}(ab_p)^2 C_p(\eta w_h) \tag{25}$$

$\{W_{\mathrm{without}} - (W_h + W_r)\}$ indicates the reduction of vibration-suppression performance, and accordingly, it indicates the influence of the energy-harvesting mechanism on suppression performance. Note that when the energy-harvesting device is used, as w_h increases $\{W_{\mathrm{without}} - (W_h + W_r)\}$ also increases. Specifically, it suggested that the total deprived power of the vibration system is reduced by η times the power of the harvested power via the diode bridge. As will be explained later, the harvested power via the diode bridge is used to drive the microprocessor for the self-powered unit. The deprived power for the energy harvesting has a significant influence on the performance of the energy-recycling vibration suppression. It should be noted that the range of w_h is constrained by the value of η in Eq. (17):

$$0 \le w_h \le \frac{1}{4(1-\eta)} \tag{26}$$

The power balance formula mentioned in Eq. (24) will be justified by the experimental data presented in Sec. IV.

III. Explanation of Digital Self-Powered Unit

A. Equations of Structure Including Piezoelectric Transducers and Controller

For the purpose of deriving generalized equations, consider an l-DOF structure having m piezoelectric transducers. The equation of motion for the structure including the piezoelectric transducers [14] can be written as

$$\mathbf{M}\ddot{\mathbf{u}} + \mathbf{D}\dot{\mathbf{u}} + \mathbf{K}\mathbf{u} = \mathbf{B}_p\mathbf{Q} + \mathbf{w} \tag{27}$$

To express Eq. (2) in vector-matrix form, the scalar equation is transformed to

$$\mathbf{V}_p = -\mathbf{B}_p^T\mathbf{u} + \mathbf{C}_p^{-1}\mathbf{Q} \tag{28}$$

In modal coordinates, the equation of motion is expressed as

$$\ddot{\boldsymbol{\xi}} + \Xi\dot{\boldsymbol{\xi}} + \Omega\boldsymbol{\xi} = \Phi^T\mathbf{B}_p\mathbf{Q} + \Phi^T\mathbf{w} \tag{29}$$

The voltage equation is written as

$$\mathbf{V}_p = -\mathbf{B}_p^T\Phi\boldsymbol{\xi} + \mathbf{C}_p^{-1}\mathbf{Q} \tag{30}$$

in which

$$\Phi \equiv [\phi_1, \phi_2, \cdots, \phi_l], \qquad \Omega \equiv \mathrm{diagonal}[\omega_k^2] \tag{31}$$

$$\Xi \equiv \mathrm{diagonal}[2\zeta\omega_k], \qquad (1 \le k \le l) \tag{32}$$

Then, Eqs. (29) and (30) can be transformed to

$$\dot{\mathbf{z}} = \mathbf{A}\mathbf{z} + \mathbf{B}\mathbf{Q} + \mathbf{E}\mathbf{w} \tag{33}$$

$$\mathbf{V}_p = \mathbf{C}\mathbf{z} + \mathbf{D}\mathbf{Q} \tag{34}$$

in which

$$\mathbf{z} \equiv [\boldsymbol{\xi}, \dot{\boldsymbol{\xi}}^T]^T, \qquad \mathbf{A} \equiv \begin{bmatrix} \mathbf{0} & \mathbf{I} \\ -\Omega & -\Xi \end{bmatrix}, \qquad \mathbf{B} \equiv \begin{bmatrix} \mathbf{0} \\ \Phi^T\mathbf{B}_p \end{bmatrix} \tag{35}$$

$$\mathbf{C} \equiv [-\mathbf{B}_p^T\Phi \quad \mathbf{0}], \qquad \mathbf{D} \equiv \mathbf{C}_p^{-1}, \qquad \mathbf{E} \equiv \begin{bmatrix} \mathbf{0} \\ \Phi^T \end{bmatrix} \tag{36}$$

If $\mathbf{Q}$ in Eq. (33) is regarded as an active-control input, the linear quadratic regulator (LQR) control theory [21] specifies that the performance index

$$J \equiv \int_0^\infty (\mathbf{z}^T\mathbf{W}_1\mathbf{z} + \mathbf{Q}^T\mathbf{W}_2\mathbf{Q})\,\mathrm{d}t \tag{37}$$

is minimized by

$$\mathbf{Q} = \mathbf{Q}_T \equiv -\mathbf{F}\mathbf{z} \tag{38}$$

in which

$$\mathbf{F} \equiv \mathbf{W}_2^{-1}\mathbf{B}^T\mathbf{P}_1 \tag{39}$$

Here, $\mathbf{W}_1$ and $\mathbf{W}_2$ are weighting matrices, and $\mathbf{P}_1$ is a positive solution of

$$\mathbf{P}_1\mathbf{B}\mathbf{W}_2^{-1}\mathbf{B}^T\mathbf{P}_1 - \mathbf{A}^T\mathbf{P}_1 - \mathbf{P}_1\mathbf{A} - \mathbf{W}_1 = \mathbf{0} \tag{40}$$

The vector $\mathbf{Q}_T$ is an evolved form of the simple scalar in Eq. (4). While $\mathbf{Q}_T$ can handle multiple transducer systems, the simple Q_T deals with only single-transducer systems. The performance index J comprises two competing factors: the first and second terms in Eq. (37). However, the method presented in this paper only refers to the polarity of $\mathbf{Q}_T$ for the switching operation, and the meaning of $\mathbf{W}_1$ and $\mathbf{W}_2$ in switching-control systems is quite different from the standard guidelines. A comprehensive discussion and interpretation of these peculiar meanings in switching controls can be found in [16].

B. Mechanics

Figure 4 shows a view of the mechanical experiment system that consists of two added masses, a pantograph-type displacement-magnification mechanism, a piezoelectric transducer (PSt 1000/10/200-VS18, Piezomechanik GmbH), piezoelectric sensors, two cantilevered beams, a vibration shaker, and an experimental platform. The pantograph-type displacement-magnification mechanism (Fig. 5), attached to the upper beam and upper side of the platform, is used to amplify the displacement. One piezoelectric sensor is attached to the base of the upper beam. Additional measuring instruments (a laser displacement sensor and a load cell) are arranged around the system. These measuring instruments are only used for recording and not used for the semi-active feedback

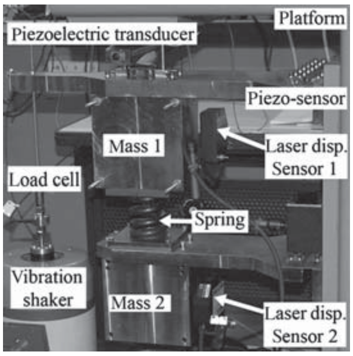

Fig. 4 View of the mechanical part in the two-DOF system; "disp." denotes displacement.

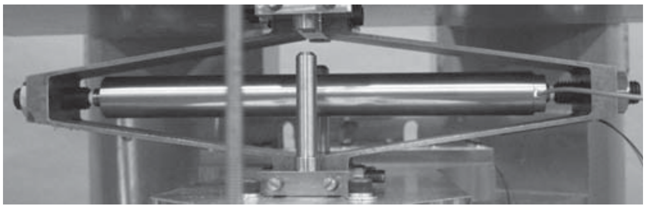

Fig. 5 Piezoelectric transducer and pantograph-type displacement-magnification mechanism.

control. For the purpose of effective analysis, an equivalent two-DOF spring-mass model is constructed for the experimental system. The natural frequencies of first and second vibration modes at constant electric charge are 20.3 and 36.6 Hz, respectively.

C. Electrics

Figure 6 shows a diagram of the energy flow and control stream of the digital self-powered system. The energy-harvesting section, consisting of four diodes, can supply the harvested energy to the microprocessor (78K0R/KE3-L, Renesas Electronics). The energy harvester, with a storage capacitor C_s, is connected to the piezoelectric transducer to collect vibrational energy. The circuit harvests electrical energy in a piezoelectric transducer attached to a vibrating structure, and it supplies energy to the energy harvester and sends the collected energy to the microprocessor. When the vibration becomes large, the harvested energy also increases, and accordingly, the processor enters a wake mode and suppresses the vibration. In contrast, when the vibration is suppressed to a very small level, the harvested energy decreases, and accordingly, the processor enters a sleep mode and waits. In this manner, the processor suppresses vibrations according to the vibrational magnitude, which is a preferable characteristic for an autonomous self-powered unit.

The processing speed and energy consumption of the processor must be finely balanced. The processor should not be too fast, or else

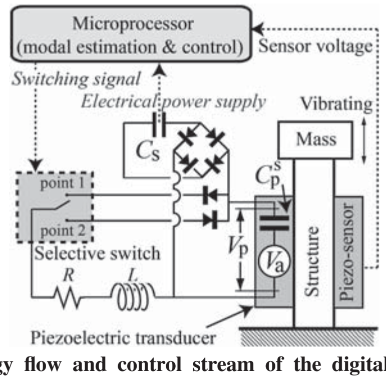

Fig. 6 Energy flow and control stream of the digital self-powered suppression system.

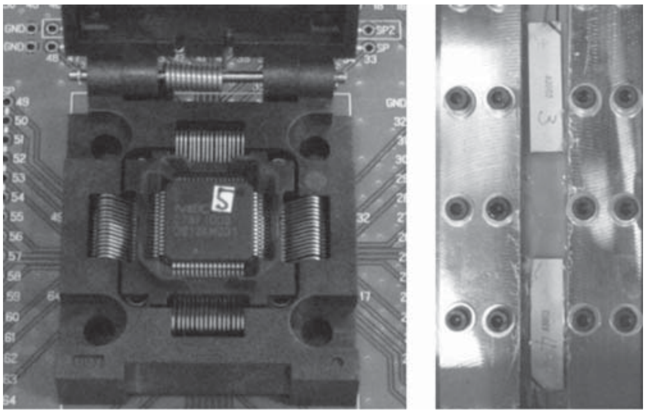

Fig. 7 Autonomous digital processor inside the digital processor board (left) and the piezoelectric sensors (right).

its energy consumption would exceed the energy harvested from the piezoelectric transducer. Conversely, a processor that is too slow would decrease the control frequency and make the system unstable. A 16-bit microprocessor has been selected that has an internal clock oscillator, RAM, flash ROM for storing programs, 10-bit A/D converters, digital output ports, a hardware integer multiplier/divider, and a real-time clock. All the necessary functions for switching control are built in. Piezoelectric sensors (C-91H, Fuji Ceramics Corporation) attached to the structure and that output a voltage that is proportional to the upper mass displacement are connected to the A/D port of the processor.

The energy supply circuit consists of a switch, diode bridge, storage capacitor, and a dc/dc converter. The diode bridge rectifies the transformed voltage, and the capacitor stores it. The dc/dc converter changes the high input value of the piezoelectric voltage into a low output voltage of 2.0 V. The $\mathrm{d}c/\mathrm{d}c$ converter transforms voltage efficiently in a low-output-current range (approximately 1–2 mA), and it is configured for the wide input piezoelectric voltage range. This wide voltage range is an advantage of the selected $\mathrm{d}c/\mathrm{d}c$ converter. Figure 7 shows the digital processor inside the CPU board and the two piezoelectric sensors.

D. Modal Estimation in Digital Processor

The structure for the experiment has multiple modal vibrations; however, a reduced modal estimation of a two-DOF system as a modal truncation has been implemented to facilitate effective estimation. To execute multimodal estimation, the Kalman filter [21] for the proposed system is derived, and vibration suppression is achieved by using the estimated values of the modal velocities and displacements. Equation (33), the equation of motion, can be transformed into

$$\dot{\mathbf{z}}_{\mathrm{ex}} = \mathbf{A}_{\mathrm{ex}}\mathbf{z}_{\mathrm{ex}} + \mathbf{B}_{\mathrm{ex}}Q + \mathbf{E}_{\mathrm{ex}}\mathbf{w}, \qquad \mathbf{z}_{\mathrm{ex}} \equiv [\xi_1, \xi_2, \dot{\xi}_1, \dot{\xi}_2]^T \tag{41}$$

The subscript ex indicates that an experimental system with modal truncation is being considered. The sensor equation can be written as

$$V_{\mathrm{sen}} = \mathbf{C}_{\mathrm{ex}}\mathbf{z}_{\mathrm{ex}} \tag{42}$$

Because the system has one transducer and one parallel sensor group, the values Q and V_{sen} are scalars. The Kalman filter for estimating $\mathbf{z}_{\mathrm{ex}}$ is

$$\dot{\hat{\mathbf{z}}}_{\mathrm{ex}} = \mathbf{A}_{\mathrm{ex}}\hat{\mathbf{z}}_{\mathrm{ex}} + \mathbf{B}_{\mathrm{ex}}Q + \Gamma_{\mathrm{ex}}(V_{\mathrm{sen}} - \mathbf{C}_{\mathrm{ex}}\hat{\mathbf{z}}_{\mathrm{ex}}) \tag{43}$$

in which the observer gain matrix Γ_{ex} is defined as

$$\Gamma_{\mathrm{ex}} \equiv \mathbf{P}_2\mathbf{C}_{\mathrm{ex}}^T\mathbf{S}_2^{-1} \tag{44}$$

Here, $\mathbf{P}_2$ is a positive definite solution of

$$\mathbf{A}_{\mathrm{ex}}\mathbf{P}_2 + \mathbf{P}_2\mathbf{A}_{\mathrm{ex}}^T - \mathbf{P}_2\mathbf{C}_{\mathrm{ex}}^T\mathbf{S}_2^{-1}\mathbf{C}_{\mathrm{ex}}\mathbf{P}_2 + \mathbf{S}_1 = \mathbf{0} \tag{45}$$

The noise covariance matrices for Eqs. (41) and (42) are $\mathbf{S}_1$ and $\mathbf{S}_2$, respectively. From Eq. (38), the estimated value of the state vector $\hat{\mathbf{z}}_{\mathrm{ex}}$ is then used to calculate the switching criteria Q_T as

$$Q_T \equiv -\mathbf{F}\hat{\mathbf{z}}_{\mathrm{ex}} \tag{46}$$

For digital implementation of the self-powered programming, a switching strategy using the switching criteria is constructed. When some of the energy harvested from the vibrations is supplied to the processor, the processor enters a wake mode. In summary, the programming code is created to implement the circuit switch determination and Kalman filter to estimate the modal velocities and displacements.

IV. Digital Self-Powered Suppression Experiments

A. Operating Procedure of Digital Processor

The digital processor 1) activates using the power supplied by the energy-harvesting section; 2) collects data pertaining to the structural vibrations from the piezoelectric sensors; 3) calculates the modal estimation using the Kalman filter; 4) calculates the switching criteria; and 5) activates the switch to inverse the voltage polarity of the piezoelectric transducer when the switching criteria polarity shifts. All of these steps are carried out in each clock cycle.

In particular, instead of the discrete Kalman filter, a continuous filter is used to update in time with the fourth-order Runge–Kutta method in the processor because this continuous formula is more precise than the discrete formula. The estimation precision is of great importance in systems subject to large ambient noise. For the purpose of constructing the controller based on the LQR theory and the modal estimator (i.e., the continuous Kalman filter), a calculation that emulates the experimental setup is performed. To measure the suppression performance

$$I_{\mathrm{rms}} \equiv \int_{t_S}^{t_E} \delta_{\mathrm{rms}}\,\mathrm{d}t \tag{47}$$

was calculated for $t_S = 0.0$ s and $t_E = 5.0$ s, in which

$$\delta_{\mathrm{rms}} \equiv \sqrt{\frac{x_1^2 + x_2^2}{2}} \tag{48}$$

First, the feedback gain matrix $\mathbf{F}$ of Eq. (46) was obtained. $\mathbf{W}_1$ was set to

$$\mathbf{W}_1 = \mathrm{diagonal}[1,\ 1,\ 1/\omega_1^2,\ 1/\omega_2^2] \tag{49}$$

and $\mathbf{W}_2$ was set to a scalar value and optimized so that I_{rms} was minimized for excited vibrations. As a result, $\mathbf{W}_2$ was set to 1.0×10^8, and accordingly, $\mathbf{F}$ was determined. Next, the observer gain Γ_{ex} of Eq. (44) was obtained. It was assumed that

$$\mathbf{S}_1 = s_1\begin{bmatrix}\mathbf{0} & \mathbf{0}\\ \mathbf{0} & \mathbf{I}_2\end{bmatrix}, \qquad \mathbf{S}_2 = s_2\mathbf{I}_4 \tag{50}$$

In the simulation, the structure was excited at two frequencies: the first and the second modes, and the state vector was estimated by the observer. To evaluate the observation performance, the estimation error

$$\int_{t_S}^{t_E} |\hat{\mathbf{z}} - \mathbf{z}|^2\,\mathrm{d}t \tag{51}$$

was calculated for $t_S = 0.0$ s and $t_E = 5.0$ s. The values of s_1 and s_2 in Eq. (50) were determined so that the error was minimized, and an observer gain was obtained with $s_1 = 1.0 \times 10^8$ and $s_2 = 1.0 \times 10^3$. Consequently, the observer of the experiment was expressed by Eq. (43).

B. Self-Powered Single-Modal Vibration Suppression

First, experiments of the single-modal vibration suppression were carried out using the digital self-powered unit. A function generator created the input force waves and relayed them to the vibration shaker. Figure 8 shows the displacement of the lower mass and voltage of the piezoelectric transducer without any control as a function of time. The vibration reached the steady-state condition. Clear sinusoidal waves can be seen in this figure; the magnitudes of displacement and the voltage are 0.630 mm and 87.2 V, respectively. Figure 9 shows the displacement and piezoelectric voltage with the digital self-powered autonomous control over time. Focusing on the displacement magnitude compared with that in Fig. 8, the displacement is reduced from 0.630 to 0.128 mm—a reduction of 79.7%. This reduction is quite significant and striking, considering that this is a completely self-powered control unit. At the positive peak displacement, the voltage polarity inverts from positive to negative, and the opposite occurs at the negative peak displacement. This voltage behavior in Fig. 9 is quite typical of the voltage inversion mechanism [12–14], and it means that none of the processing procedures, from modal estimation to activation of the switch, suffer from any time delay. The overshoot ratio of Eq. (12) is around 61%, which indicates that the circuit was close to optimal in practice. After inversion, the piezoelectric voltage increased in proportion to the displacement attributable to the piezoelectric effect, and reached a plateau where both the harvested and consumed power in the device was balanced.

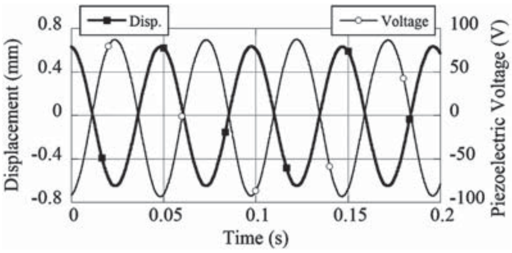

Fig. 8 Experimental results of the displacement and piezoelectric voltage in the single-modal vibration system under vibration excitation without control; "disp." denotes displacement.

To evaluate the suppression performance as a function of vibration strength, four cases of single-modal vibration excitations were examined. The input force for the vibration shaker is expressed with β and γ as

$$\gamma\left\{\beta\sin(\omega_1 t) + \frac{11}{7}(1-\beta)\sin(\omega_2 t)\right\} \tag{52}$$

in which ω_1 and ω_2 are the angular frequencies of first and second vibration modes, respectively; β is the modal combination parameter; and γ is the magnitude of vibration excitation. A vibration excitation with $\beta = 1$ indicates excitation with only the first mode, and the vibration excitation with $\beta = 0$ indicates excitation with only the second mode. In the experiment, γ was set to 0.7 and 0.42 V. The coefficient of the second mode [i.e., $11/7$ in Eq. (52)] was chosen so that the first and second modes had the same displacement magnitude for each input. Table 1 lists the four single-modal vibration cases with the corresponding β and γ values. The power balance for the four experimental cases is given in Table 2. The excitation power through the vibration shaker W_{excited} is calculated with the displacement and load values that were measured by the displacement sensors and the load cell. The harvested power to the diode bridge in Eq. (14), W_h, is

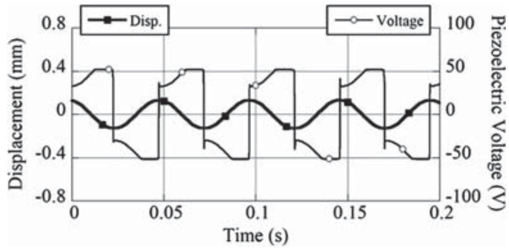

Fig. 9 Experimental results of the displacement and piezoelectric voltage in the single-modal vibration system under vibration excitation with self-powered control; "disp." denotes displacement.

Table 1 Single-modal vibration

			Shaker voltage input	
Case	β	γ	First mode	Second mode
A	0	0.35	0	0.55
B	0	0.70	0	1.1
C	1	0.35	0.35	0
D	1	0.70	0.70	0

measured with the current and voltage in the circuit. The term $\{W_{\mathrm{excited}} - (W_h + W_r)\}$ is regarded as the mechanical dissipation energy as a result of the mechanical-damping mechanism. Table 2 shows that the normalized value, $\{1 - (W_h + W_r)/W_{\mathrm{excited}}\}$, is almost the same for each modal excitation in spite of the different γ values. It is quite reasonable that the dissipation is an inherently constant value of the modal damping, regardless of vibration amplitude. In general, electronic devices employed in experiments have some nonlinearities that are difficult to measure precisely to create an accurate mathematical model. In spite of these actual difficulties, it is possible to say that the theoretical analysis in Sec. II might be justified practically without substantial discrepancy.

C. Self-Powered Multimodal Vibration Suppression

Multimodal vibration-suppression experiments were also carried out using the digital self-powered system. Figure 10 shows the multimodal vibration suppression with $\beta = 0.5$ and $\gamma = 0.7$. The switching timing (at the time of voltage inversion) is adaptive to the vibrational state. This is quite important for sophisticated vibration suppression because sensitive and adaptive switching can simultaneously suppress multiple-mode vibrations, unlike monotone switching at equally spaced intervals. Furthermore, the piezoelectric voltage appears to keep a high value because the switching timing is appropriate to avoid unnecessary energy dissipation. This high voltage value leads to high performance of vibration suppression, which is quite a preferable suppression system.

To compare the suppression performance of the digital self-powered system and an analog system, an analog control emulator has been fabricated that simulates analog self-powered systems with an external energy supply. Because actual self-powered analog-directive controllers [8–10] have a large amount of energy dissipation in resistors, a fair comparison between analog self-powered systems and the digital self-powered system was thought to be difficult to carry out practically. For the purposes of impartial comparison, an analog controller was constructed by a PC that implemented the derivative control in Eq. (4). The analog controller emulated by the PC has no time delay and no energy consumption, which provide an ideal controller. The analog control emulator does not consume any harvested energy to drive its controller, and thus, is highly advantageous over the digital self-powered system in terms of energy dissipation. Figure 11 shows the ratio $\delta^2_{\mathrm{rms}}/W_{\mathrm{excited}}$ for various β and γ values. The ratio values are normalized to the value of the excitation case: digital self-powered case with $\gamma = 0.7$. The figure clearly shows that the analog system cannot suppress complicated vibrations [i.e., a combination of two vibration modes, especially in which $(0.1 < \beta < 0.6)$], whereas the digital system is able to suppress multimodal vibrations sufficiently. This confirms, in spite of the high advantages of analog-emulated controllers, the superiority of the proposed digital unit over conventional analog systems for combined vibration suppression.

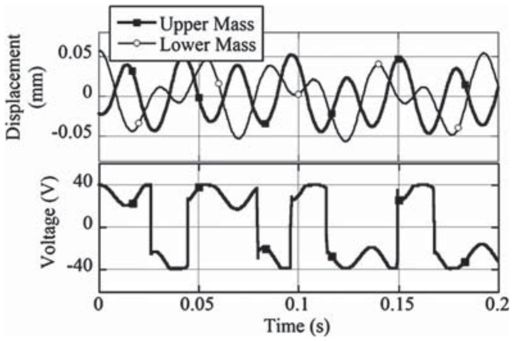

Fig. 10 Experimental results of the displacement and piezoelectric voltage for multimodal vibration suppression.

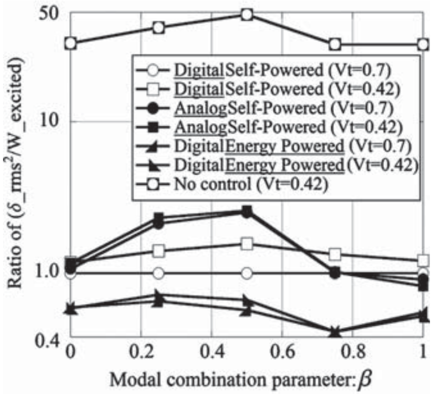

Fig. 11 Comparison of $\delta^2_{\mathrm{rms}}/P_{\mathrm{excited}}$ for various vibration-suppression methods.

V. Discussions on Advantages of Digital Self-Powered Autonomous System

The proposed digital self-powered autonomous system affords several significant advantages over conventional systems.

First, unlike typical analog self-powered systems [8–10], the proposed system is programmable and can thus be easily used to implement any type of control scheme and properly tune various parameters. Analog-circuit systems cannot accomplish advanced modern control schemes (e.g., linear quadratic Gaussian and H-infinity controls); however, the digital system easily enables any sophisticated control scheme and will implement any advanced filtering algorithm. Therefore, this autonomous system is applicable even to complex multi-input/multi-output systems.

Second, this proposed unit possesses the same advantages as semi-active methods in that it has a highly effective performance and excellent stability (with no chance of spillover instability), thus affording good control reliability in practice. This characteristic results in much utilization for the structures whose mathematical model errors are inevitable to avoid, such as large structures, plants constructed in space or deep-ocean.

Third, the proposed self-powered unit can ubiquitously be used at any site and even at sites without external power. Many structures in sparsely settled regions are subject to vibrations, and conventional suppression systems cannot be used, as there is no access to an external power supply. It is because of considerations such as energy saving and actual difficulties involved in wiring, such as in space structures, moving vehicles, long bridges, constantly streaming factory walls, and acoustically insulated walls alongside highways

Table 2 Input and dissipation power balance in the self-powered system (values in milliwatts)

Case	W_{excited}	W_h	W_r	$W_{\mathrm{excited}} - (W_h + W_r)$	$1 - (W_h + W_r)/W_{\mathrm{excited}}$
A	15.99	8.47	5.39	2.13	0.133
B	51.08	17.9	26.4	6.74	0.132
C	22.27	8.50	7.39	6.39	0.287
D	74.07	1708	34.5	21.8	0.294

and high-speed railroads, that conventional suppression systems cannot be used. Because the digital self-powered vibration suppressor is autonomous, multifunctional, and easily adaptable to various applications, the authors strongly expect that it will find many practical applications in automatically controlling various structural vibrations.

Last, the authors describe the limitation of the digital self-powered system. As mentioned in this paper, any electronic device (e.g., a microprocessor or a dc/dc converter) requires some amount of electrical energy to drive. While the stored energy is below the required amount, the total system is unable to run. When the vibration becomes large, the harvested energy also increases, and accordingly, the processor enters a wake mode and starts to suppress the vibration. In contrast, when the vibration is suppressed to a very small level, the processor enters a sleep mode. The boundary of these wake-up and sleep modes indicates the system's limitation, in other words, the dead band of vibrations. The dead band of vibrations is directly linked with the consumption energy of electronic components. It can be said that the behavior (i.e., these wake-up and sleep modes) depending on the vibration amplitude is quite reasonable as an autonomous vibration suppressor. Considering that some amount of the stored energy is needed to drive a microprocessor, the digital self-powered unit may not handle impulsive shocks well because of the lack of driving energy, while it can handle continuous vibrations beautifully.

Furthermore, developmental applications of the invented device are mentioned. Because the energy-harvesting mechanism is inherently contained in the total system, the digital self-powered unit can be used as an autonomous energy harvester (or an autonomous power scavenger). Such an autonomous energy harvester has a great potential for realizing a wireless-network-type structural health monitoring (SHM) system. When it comes to isolated structures, moving vehicles, and rotating devices, such as turbine blades and automobile tires, the autonomous digital self-powered unit is suitable for a simple wireless SHM system having a built-in energy harvester.

VI. Conclusions

A digital self-powered autonomous vibration suppressor with a microprocessor has been proposed. The digital and autonomous approach enables the vibration suppressor to be programmed, and thus, is versatile in control schemes. Vibration-suppression experiments using the digital self-powered system indicated that the vibration magnitude reduced dramatically by as much as 79.7%. Moreover, the theoretical formula for the power balance was verified with the experimental data. Multimodal vibration suppression demonstrated the adaptability of the system to suppressing complicated vibrations, and the digital autonomous unit was shown to have significant advantages over conventional analog devices. The proposed device is versatile and applicable to a variety of machines and devices. The system is useful for various applications in which energy-saving or energy-shortage concerns exist, such as large space structures, artificial satellites, and isolated lunar bases, which all are vulnerable to long nighttimes without solar power. It is hoped that the system will serve as a starting point for further innovation.

Acknowledgment

This research was supported by Grant-in-Aid for Young Scientists (A) (number 23686125) from the Japan Society for the Promotion of Science.

References

[1] Kauffman, J. L., and Lesieutre, G. A., "A Low-Order Model for the Design of Piezoelectric Energy Harvesting Devices," *Journal of Intelligent Material Systems and Structures*, Vol. 20, No. 5, 2009, pp. 495–504.
doi:10.1177/1045389X08101559

[2] Spadoni, A., Ruzzene, M., and Cunefare, A., "Vibration and Wave Propagation Control of Plates with Periodic Arrays of Shunted Piezoelectric Patches," *Journal of Intelligent Material Systems and Structures*, Vol. 20, No. 8, 2009, pp. 979–990.
doi:10.1177/1045389X08100041

[3] Min, J. B., "Flutter and Response Studied for a Mistuned Bladed Disk with Structural and Aerodynamic Coupling," *Research and Technology (NASA John H. Glenn Research Center at Lewis Field)*, 2005, pp. 156–157.

[4] Karami, M. A., and Inman, D. J., "Analytical Modeling and Experimental Verification of the Vibrations of the Zigzag Micro-Structure for Energy Harvesting," *Journal of Vibration and Acoustics*, Vol. 133, No. 1, 2011, Paper 011002.
doi:10.1115/1.4002783

[5] Erturk, A., and Inman, D. J., "An Experimentally Validated Bimorph Cantilever Model for Piezoelectric Energy Harvesting from Base Excitations," *Smart Materials and Structures*, Vol. 18, No. 2, 2009, pp. 1–18.
doi:10.1088/0964-1726/18/2/025009

[6] Knight, R. R., Mo, C., and Clark, W. W., "MEMs Interdigitated Electrode Pattern Optimization for a Unimorph Piezoelectric Beam," *Journal of Electroceramics*, Vol. 26, Nos. 1–4, 2011, pp. 14–22.
doi:10.1007/s10832-010-9621-8

[7] Hagood, N. W., and von Flotow, A., "Damping of Structural Vibrations with Piezoelectric Materials and Passive Electrical Networks," *Journal of Sound and Vibration*, Vol. 146, No. 2, 1991, pp. 243–268.
doi:10.1016/0022-460X(91)90762-9

[8] Niederberger, D., and Morari, M., "An Autonomous Shunt Circuit for Vibration Damping," *Smart Materials and Structures*, Vol. 15, No. 2, 2006, pp. 359–364.
doi:10.1088/0964-1726/15/2/016

[9] Lallart, M., and Guyomar, D., "An Optimized Self-Powered Switching Circuit for Non-Linear Energy Harvesting with Low Voltage Output," *Smart Materials and Structures*, Vol. 17, No. 3, 2008, Paper 035030.
doi:10.1088/0964-1726/17/3/035030

[10] Onoda, J., "Some Advances in Energy Recycling Semiactive Vibration Suppression," *Advances in Science and Technology*, Vol. 56, 2008, pp. 345–354.
doi:10.4028/www.scientific.net/AST.56.345

[11] Onoda, J., and Makihara, K., "Performance of Simple and Sophisticated Control in Energy-Recycling Semi-Active Vibration Suppression," *Journal of Vibration and Control*, Vol. 14, No. 3, 2008, pp. 417–436.
doi:10.1177/1077546307080027

[12] Richard, C., Guyomar, D., Audigier, D., and Bassaler, H., "Enhanced Semi Passive Damping Using Continuous Switching of a Piezoelectric Device on an Inductor," *Proceedings of the SPIE Smart Structures and Materials Conference*, Vol. 3989, Society of Photo-Optical Instrumentations Engineers, Bellingham, WA, 2000, pp. 288–299.

[13] Corr, L. R., and Clark, W. W., "A Novel Semi-Active Multi-Modal Vibration Control Law for a Piezoceramic Actuator," *Journal of Vibration and Acoustics*, Vol. 125, No. 2, 2003, pp. 214–222.
doi:10.1115/1.1547682

[14] Onoda, J., Makihara, K., and Minesugi, K., "Energy-Recycling Semi-Active Method for Vibration Suppression with Piezoelectric Transducers," *AIAA Journal*, Vol. 41, No. 4, 2003, pp. 711–719.
doi:10.2514/2.2002

[15] Lefeuvre, E., Badel, A., Richard, C., and Guyomar, D., "High Performance Piezoelectric Vibration Energy Reclamation," *Proceedings of the SPIE Smart Structures and Materials Conference*, Vol. 5390, Society of Photo-Optical Instrumentations Engineers, Bellingham, WA, 2004, pp. 379–387.

[16] Makihara, K., Onoda, J., and Minesugi, K., "Comprehensive Assessment of Semi-Active Vibration Suppression Including Energy Analysis," *Journal of Vibration and Acoustics*, Vol. 129, No. 1, 2007, pp. 84–93.
doi:10.1115/1.2345675

[17] Shimose, S., Makihara, K., Minesugi, K., and Onoda, J., "Assessment of Electrical Influence of Multiple Piezoelectric Transducers' Connection on Actual Satellite Vibration Suppression," *Smart Materials Research*, Vol. 2011, 2011, Paper 686289.
doi:10.1155/2011/686289

[18] Qiu, J., Ji, H., and Zhu, K., "Semi-Active Vibration Control Using Piezoelectric Actuators in Smart Structures," *Frontiers of Mechanical Engineering in China*, Vol. 4, No. 3, 2009, pp. 242–251.
doi:10.1007/s11465-009-0068-z

[19] Jaffe, B., Cook, W. R., Jr., and Jaffe, H., *Piezoelectric Ceramics*, Academic Press, London, 1979, pp. 16–20.

[20] Balas, M. J., "Direct Velocity Feedback Control of Large Space Structures," *Journal of Guidance, Control, and Dynamics*, Vol. 2, No. 3, 1979, pp. 252–253.
doi:10.2514/3.55869

[21] Kwakernaak, H., and Sivan, R., *Linear Optimal Control System*, Wiley-Interscience, New York, 1972, pp. 220–222, 339–346.

R. Ohayon
Associate Editor

電力自立型の高機能振動制御装置

― 外部電源が一切不要 ―

槙原 幹十朗

東北大学 大学院工学研究科
航空宇宙工学専攻 准教授

槙原　幹十朗（まきはら かんじゅうろう）

略歴

1. 学士（工学） 東京大学 1998
2. 修士（工学） 東京大学 2000
3. 博士（工学） 東京大学 2004

（注）2002年一年間、東京大学・研究交換留学生としてウィーン工科大学に留学。

① 宇宙航空研究開発機構(JAXA) 宇宙科学研究本部(ISAS)
② ケンブリッジ大学・英国
③ 宇宙航空研究開発機構(JAXA) 宇宙科学研究所(ISAS)
④ 東北大学　大学院工学研究科　航空宇宙工学専攻　2011年1月より

圧電素子を用いたエネルギ回生型セミアクティブ（準能動的）制振

研究の背景 (1/2)

- 準能動的制振

1. 振動を抑えるように系の状態を制御する。
2. 受動的エネルギー散逸メカニズムを用いる。
3. 系にエネルギーを与えない。
4. 常に安定である。
5. 一般に、準能動的制振の性能は能動的制振の性能に比べ低い。

研究の背景 (2/2)

- 振動している構造物からエネルギーを奪う事で、制振（振動制御・抑制）を行っている。
- 準能動的制振の性能を向上させるために、このエネルギーを回収し、効果的に用いることができないだろうか？

⇩

エネルギー回生型準能動的制振

- 系にエネルギーを与えない。

⇩

準能動的制振の安定性は保持される。

圧電トランスデューサを組み込んだ トラス構造物の運動方程式

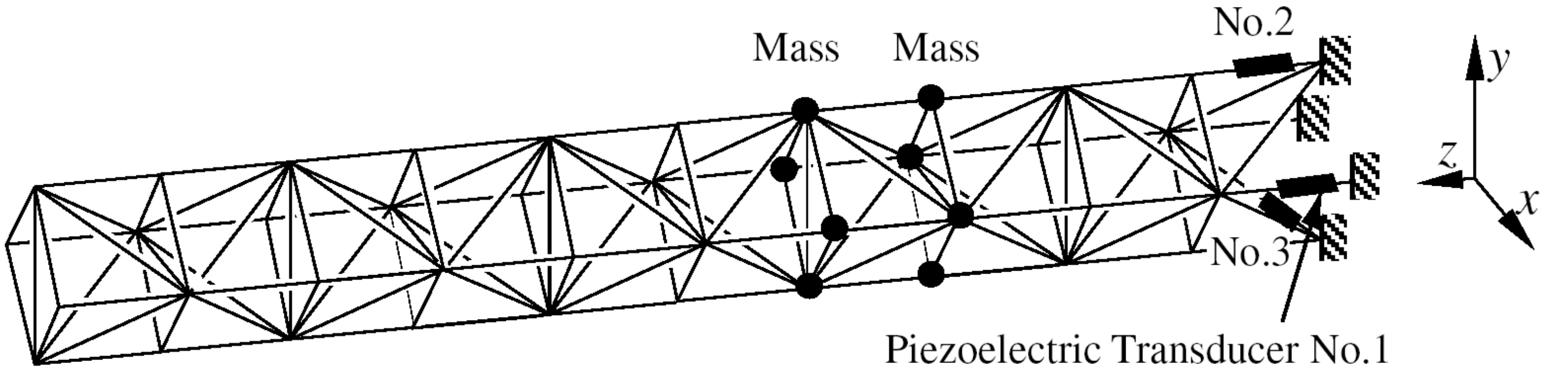

$$M\ddot{\vec{x}} + K\vec{x} = \vec{f} + B_1\vec{Q}$$

$$\vec{V} = -B_1{}^T\vec{x} + C^{-1}\vec{Q}$$

$\vec{Q}$: 電荷ベクトル (**制御量**)

$\vec{V}$: 電圧ベクトル(こちらを制御量としても良い：多彩な定式化)

圧電トランスデューサのモデルと電気回路

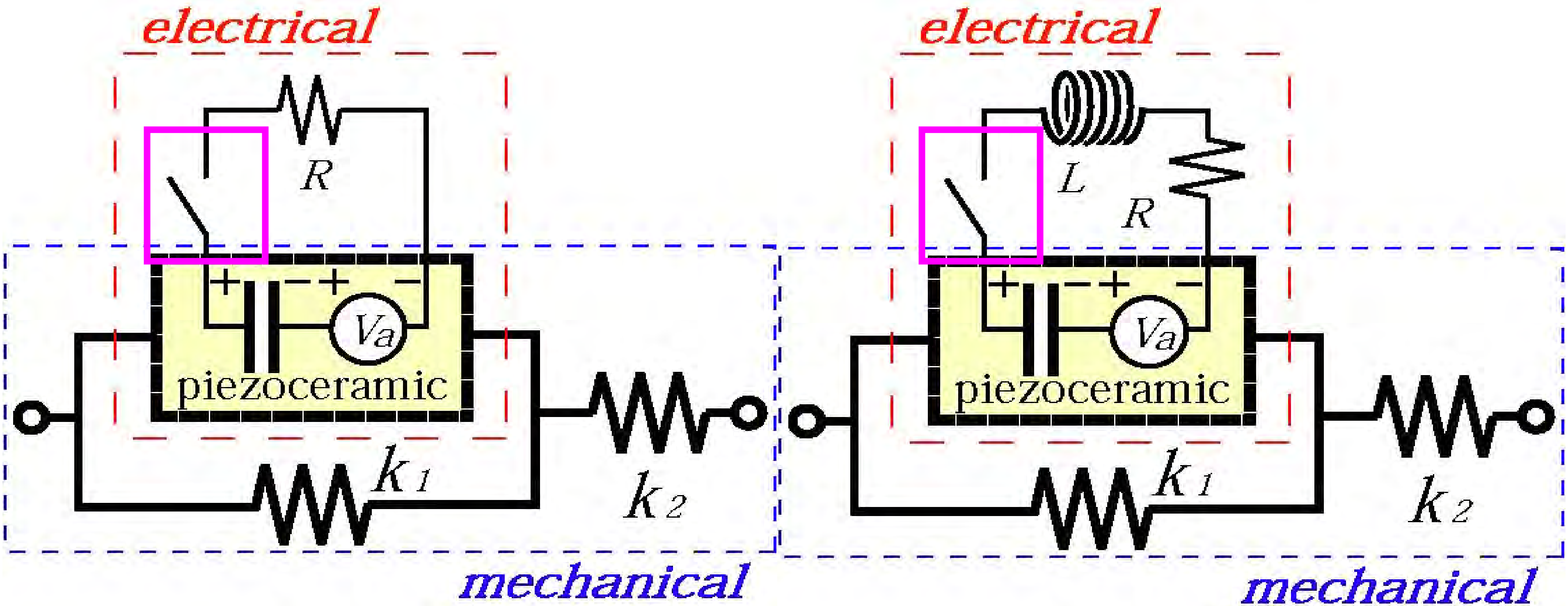

従来制御 R-switching　　エネルギ回生型 LR-switching

- 準能動的制振を目指すので、スイッチのみを制御する。

圧電トランスデューサを組み込んだ構造物の振動制御

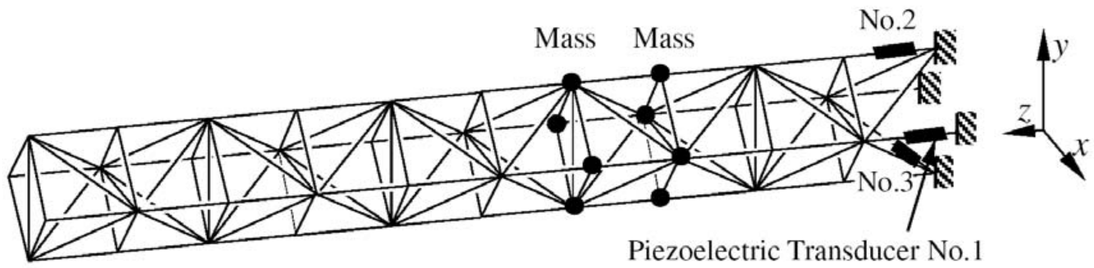

$$M\ddot{\vec{x}} + K\vec{x} = \vec{f} + B_1\vec{Q}$$

$$\vec{V} = -B_1{}^T\vec{x} + C^{-1}\vec{Q}$$

$\vec{Q}$: 電荷ベクトル (制御量)

- もしも、系を能動的に制御できるのであれば、あらゆる能動制御理論を用いる事ができる。
  その場合、$\vec{Q} = \boxed{\vec{Q}_T}$(最適制御量)

- 制御量ベクトル $\vec{Q}$ の成分の絶対値が大きい程、制振効果は一般に高い。電圧が高くても，効果は高い

エネルギー回生型制振手法(LR-switching) と 従来型制振手法 (R-switching)

従来型(R-switching)

- 回路 A を用いる.
- スイッチをオンした後，電圧の値は，0に漸近する.
- 電圧の符号を反転出来ない.

エネルギー回生型(LR-switching)

- 回路 B を用いる.
- スイッチをオンした後，電圧の値は振動する.
- 電圧の符号を反転出来る.

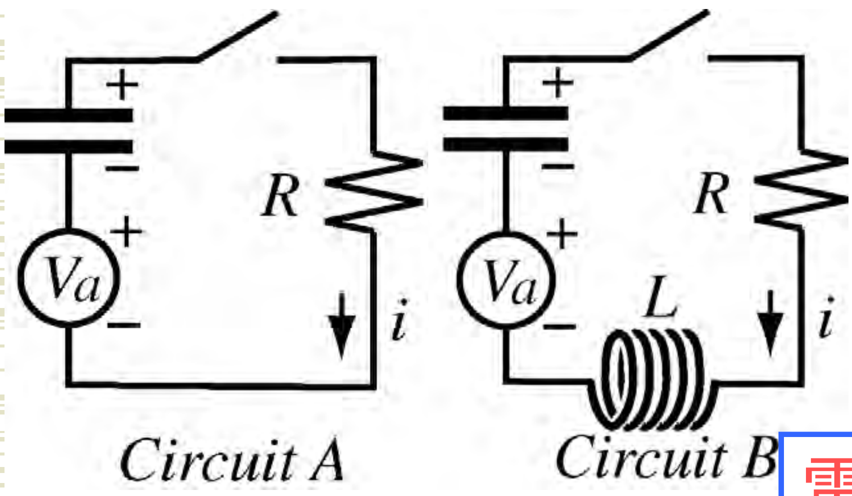

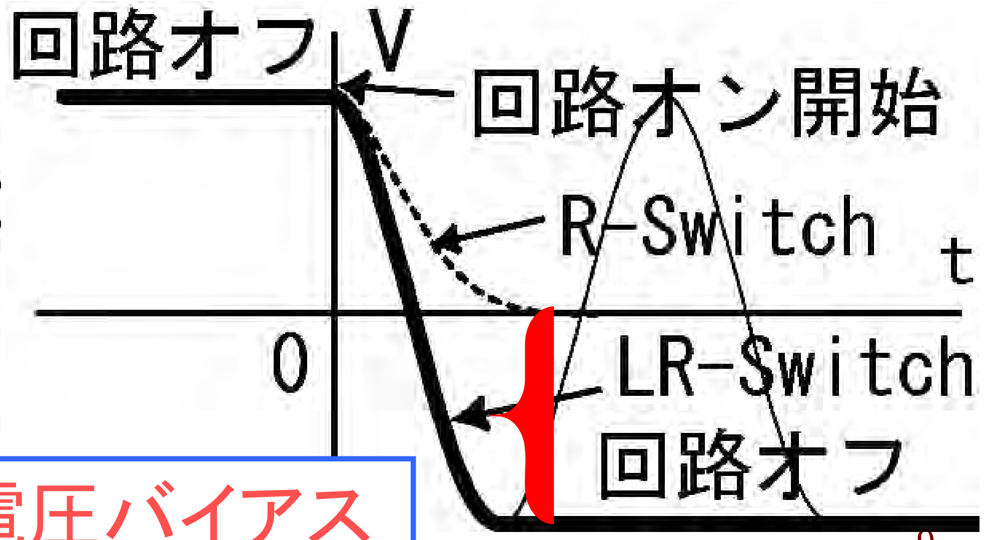

電圧バイアス

エネルギー回生型制振手法(LR-switching)と従来型制振手法(R-switching)の概念図

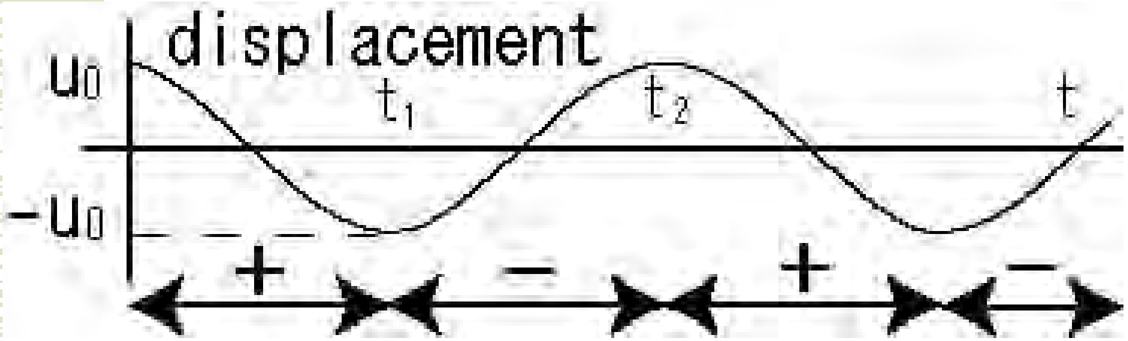

Polarity of the target value VT

$$\underline{V} = C^{-1}\underline{Q} - b\,\underline{u}$$

電圧　電荷　変位

$$Q = CV + bCu$$

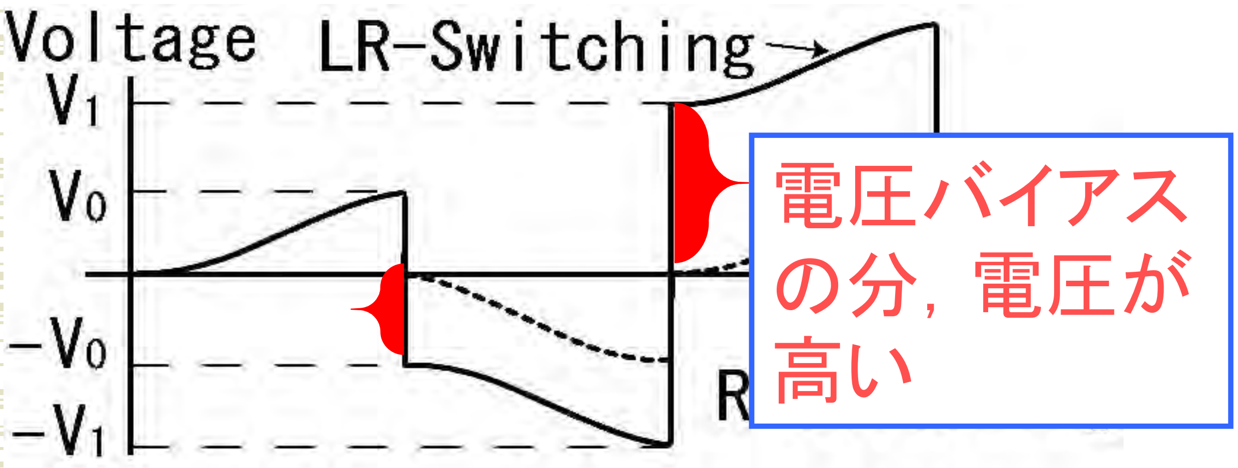

エネルギー回生型では，電荷・電圧が増大する.

従来型では電圧値は一定.

制振実験写真 (1/2)

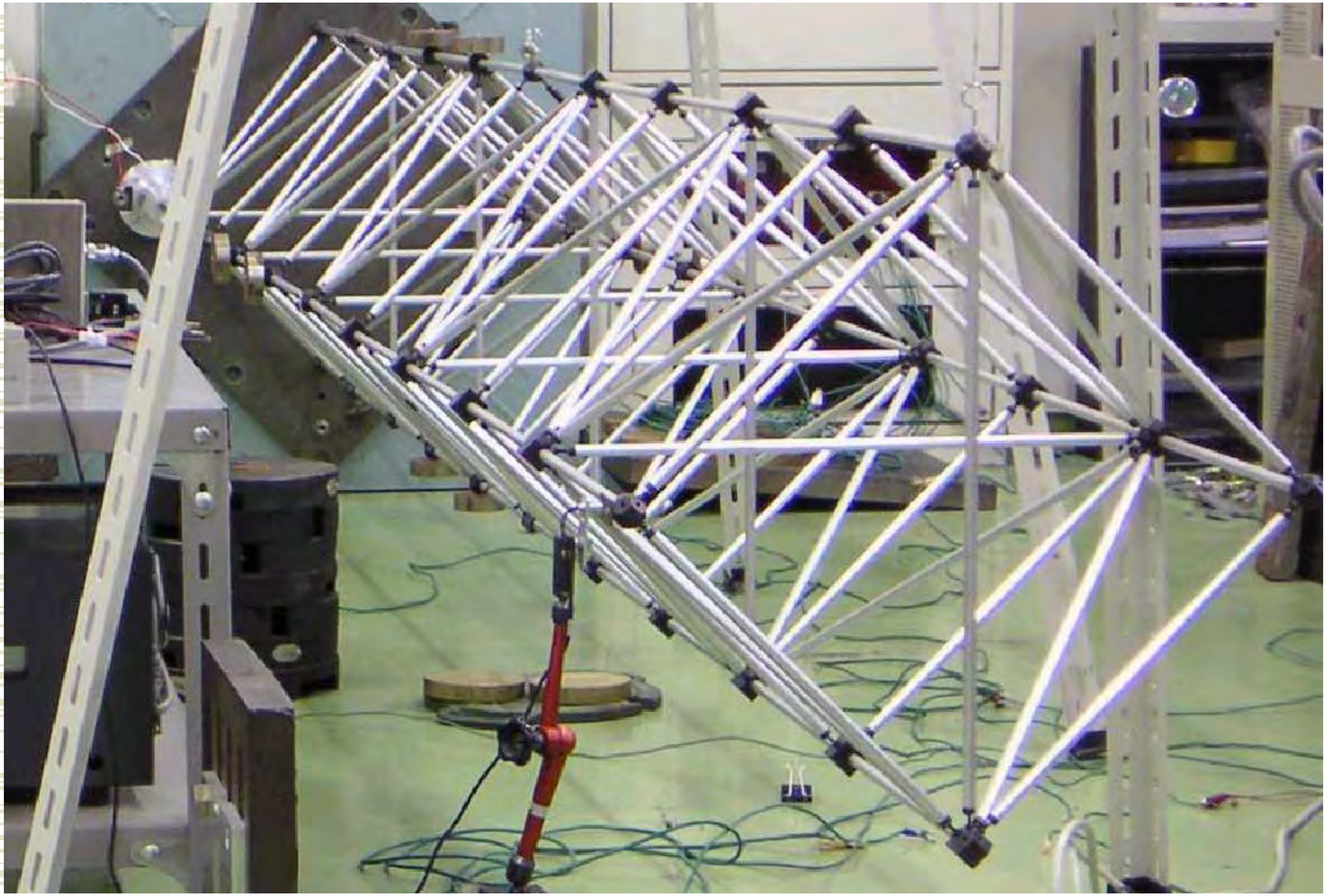

制振実験写真 (2/2)

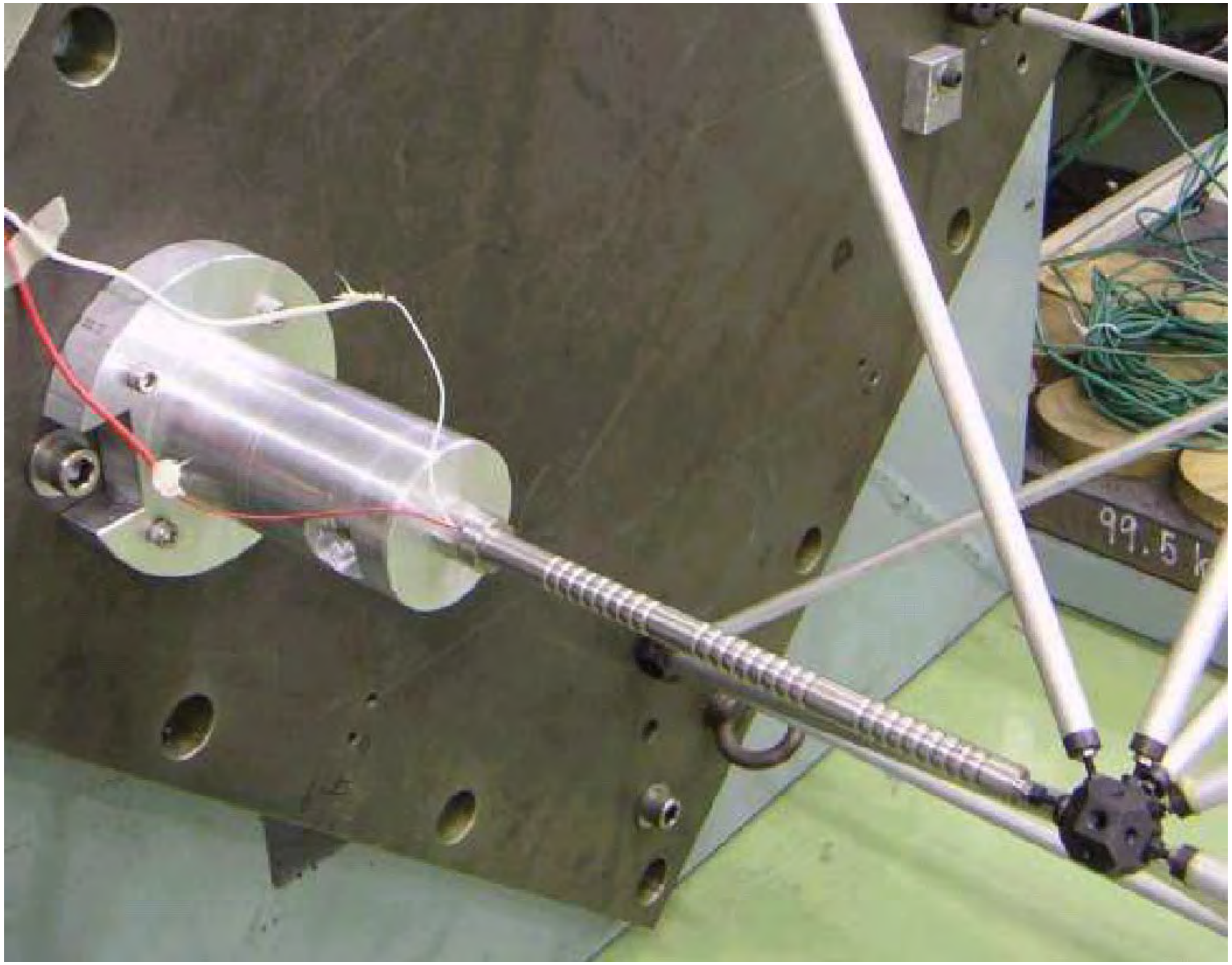

バイアスの効果：自由振動中の振動制御実験

バイアスだけで，振動制御の効果が驚くほど異なる．

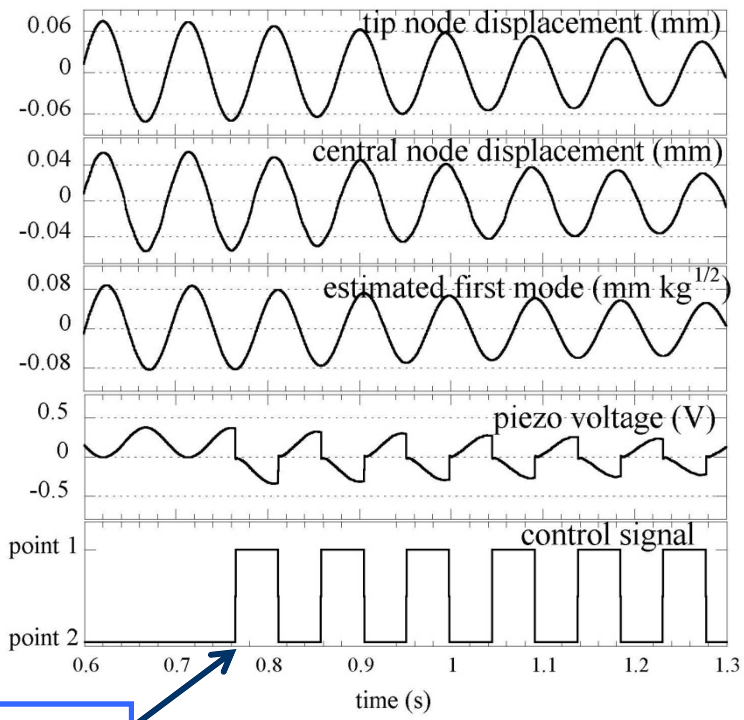

制御開始

バイアスなし

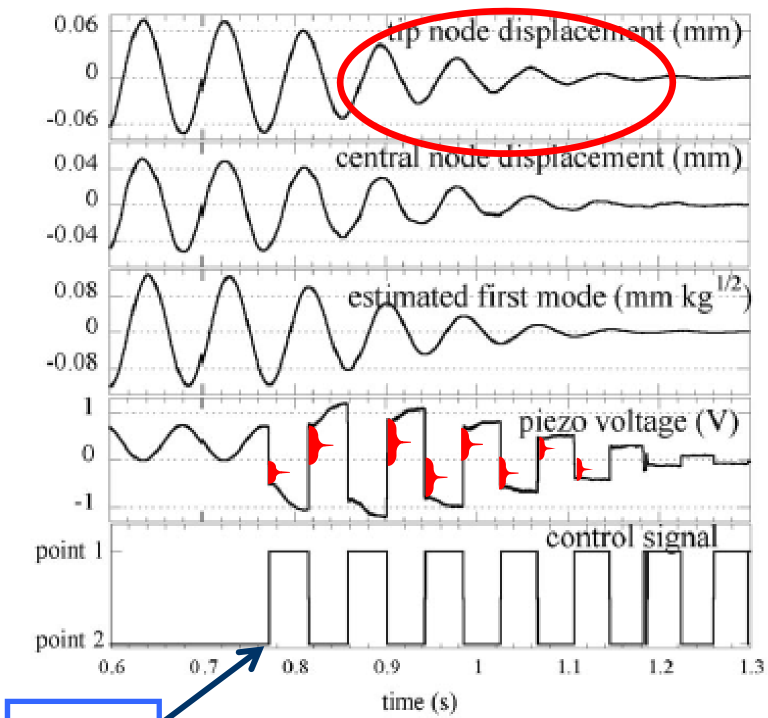

制御開始

バイアスあり